Chem Biol Drug Des 2015; **85:** 549–564

Research Article

Repurposing Human PDE4 Inhibitors for Neglected Tropical Diseases. Evaluation of Analogs of the Human PDE4 Inhibitor GSK-256066 as Inhibitors of PDEB1 of *Trypanosoma brucei*

Stefan O. Ochiana[1], Nicholas D. Bland[2], Luca Settimo[1], Robert K. Campbell[2] and Michael P. Pollastri[1]*

[1]Department of Chemistry and Chemical Biology, Northeastern University, 417 Egan Research Center, 360 Huntington Avenue, Boston, MA 02115, USA
[2]Marine Biological Laboratory, Josephine Bay Paul Center for Comparative Molecular Biology and Evolution, 7 MBL Street, Woods Hole, MA 02543, USA
**Corresponding author: Michael P. Pollastri, m.pollastri@neu.edu*

Cyclic nucleotide phosphodiesterases (PDEs) have been identified as important enzyme targets for drug development in both humans and *Trypanosoma brucei,* the causative agent of human African trypanosomiasis. With this in mind, we recently reported the profiling of a range of human phosphodiesterase inhibitors, showing that human PDE4 inhibitors tend to display the best potency against the trypanosomal phosphodiesterase TbrPDEB1. Among these was GSK-256066, a potent inhibitor of human PDE4 and a weak inhibitor of TbrPDEB1. In this report, we describe the results of a structure–activity relationship study of this chemotype, leading to the discovery of analogs with improved potency against TbrPDEB1 and micromolar inhibition of *T. brucei* cellular growth. We rationalize the potency trends via molecular docking of the new inhibitors into a recently reported *apo* structure of TbrPDEB1. The studies in this article will inform future efforts in repurposing human PDE inhibitors as antitrypanosomal agents.

Key words: GSK-256066, phosphodiesterase inhibitors, *TbrPDEB1*, *TbrPDEB2*, *Trypanosoma brucei*

Abbreviations: COPD, chronic obstructive pulmonary disease; HAT, human African trypanosomiasis; hPDE, human phosphodiesterase; NECT, nifurtimox/eflornithine combination therapy; TbrPDEB1, TbrPDEB2, *Trypanosoma brucei* phosphodiesterase B1 or B2.

Received 25 July 2014, revised 22 September 2014 and accepted for publication 24 September 2014

Human African trypanosomiasis (HAT) is a neglected tropical disease that affects approximately 10 000 patients in sub-Saharan Africa (1). Caused by the protozoan parasite *Trypanosoma brucei*, the advanced stage of HAT consists of an infection of the central nervous system, a condition that is invariably fatal if untreated. Current treatments for the CNS stage of HAT are suboptimal, including eflornithine (alone, or now in combination with nifurtimox) (2), which is only active against the *T. brucei gambiense* subspecies, and melarsoprol, which is a toxic organoarsenical agent whose toxicity is such that approximately 5% of patients will die from its side-effects (3).

As HAT affects some of the poorest patients in the world, there is little financial incentive to pursue costly *de novo* drug discovery programmes. With this in mind, we have applied a target repurposing approach to therapeutics discovery, wherein essential parasite targets and pathways are matched with druggable human homologs that have existing chemical matter that targets them (4). These compounds can provide new leads for antiparasitic drug discovery without undertaking a costly high-throughput screening campaign. We have pursued this approach with a variety of kinase (5,6) and phosphodiesterase (PDE) inhibitors (7–10).

Phosphodiesterase inhibitors have been developed for a variety of indications, including treatment of erectile dysfunction and pulmonary hypertension (PDE5), and chronic obstructive pulmonary disease (PDE4). The success of these efforts is evident in the approval of various selective PDE inhibitors for clinical use (11–14). *Trypanosoma brucei* expresses five PDEs, including the homologs TbrPDEB1 and B2, which have been together demonstrated to be essential by RNAi, such that both enzymes must be inhibited to affect parasite survival (15). These two enzymes are highly homologous (88.5%) (15), and we have shown previously (7) (and within this work) that inhibitors tested against both enzymes most frequently display similar potency against both. Furthermore, the essentiality data and sequence similarity between human and trypanosomal PDEs led us to believe that target repurposing could be a fruitful approach for new inhibitor discovery (7).

 doi: 10.1111/cbdd.12443

We previously reported the assessment of a range of established human PDE chemotypes against TbrPDEB1 and B2, and reported that these enzymes are susceptible to a number of chemotypes, primarily derivatives of established human PDE4 (hPDE4) inhibitors (Figure 1). Besides piclamilast (**1**) and cilomilast (**2**), we also identified GSK-256066 (**3**)(16), an investigational compound for chronic obstructive pulmonary disease (COPD), as a weak inhibitor of TbrPDEB1 (7).

Besides improving potency at the trypanosomal target, another significant issue for any target repurposing programme is to identify divergent structure–activity relationships (SAR) between the host and pathogen enzymes. Such selectivity is important to reduce potentially troublesome side effect profiles, such as emesis, as observed with most hPDE4 inhibitors, which has been a significant challenge to date (7,17).

Material and Methods

TbrPDEB1 Biochemical assay

Biochemical assays were performed as previously described (7) and are described in detail in the Supporting Information (Appendix S1). Biological assay data and chemical structures are available in Appendix S1 and as a publically shared data set at www.collaborativedrugdiscovery.com.

Human PDE4B biochemical assay

This assay was performed at Takeda Pharmaceuticals using methods previously reported (18).

Trypanosome cell culture assays

Bloodstream forms of *Trypanosoma brucei brucei* strain 427 were grown at 37 °C in a 5% CO_2 atmosphere in HMI-11 medium supplemented with 10% fetal bovine serum (FBS, Sigma). Cells in the mid-logarithmic stage of growth were diluted to a density of 10^4 cells/mL and were incubated with a range of concentrations of inhibitor in DMSO or DMSO alone. The final concentration of DMSO was 1%. Cell densities were determined after 48 h using Alamar blue (Invitrogen, Carlsbad, CA, USA) per the manufacturer's instructions. All values are the mean of three or more independent experiments.

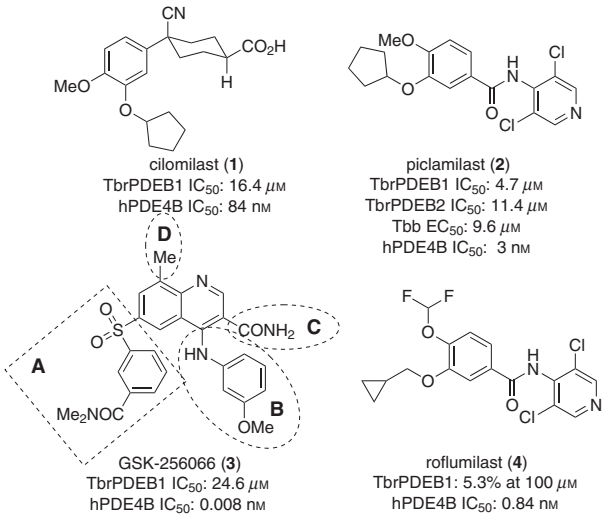

Figure 1: Previously benchmarked human PDE4 inhibitors (7,16,31,32).

Chemical Synthesis

Unless otherwise noted, reagents were obtained from Sigma-Aldrich, Inc. (St. Louis, MO, USA), Fisher Scientific, Frontier Scientific Services, Inc. (Newark, DE, USA), Matrix Scientific (Columbia, SC, USA), and used as received. Boronic acids/esters and aniline reagents were purchased, except for the boronates listed in the Supporting Information (Appendix S1). Reaction solvents were purified by passage through alumina columns on a purification system manufactured by Innovative Technology (Newburyport, MA, USA). Microwave reactions were performed using a Biotage Initiator-8 instrument. NMR spectra were obtained with Varian NMR systems, operating at 400 or 500 MHz for ^{1}H acquisitions as noted. LCMS analysis was performed using a Waters Alliance reverse-phase HPLC, with single-wavelength UV–visible detector and LCT Premier time-of-flight mass spectrometer (electrospray ionization). All newly synthesized compounds that were submitted for biological testing were deemed >95% pure by LCMS analysis (UV and ESI-MS detection) prior to submission for biological testing. Preparative LCMS was performed on a Waters FractionLynx system with a Waters MicroMass ZQ mass spectrometer (electrospray ionization) and a single-wavelength UV–visible detector, using acetonitrile/H_2O gradients with 0.1% formic acid. Fractions were collected on the basis of triggering using UV and mass detection. Yields reported for products obtained by preparative HPLC represent the amount of pure material isolated; impure fractions were not repurified.

Ethyl 6-iodo-8-methyl-4-oxo-1,4-dihydroquinoline-3-carboxylate (6)

To 4-iodo-2-methylaniline (**5a**) (5.35 g, 22.96 mmol) was added diethyl 2-(ethoxymethylene)malonate (5.10 mL, 25.3 mmol), and the reaction mixture was heated at 100 °C for 1 h. The heat was removed, and the white solid that formed was collected, washed with cyclohexane (70 mL) and ethanol 30 mL (2×), and dried in vacuo at 40 °C overnight to give diethyl 2-(((4-iodo-2-methylphenyl)amino)methylene)malonate (Yield: 98%). ^{1}H NMR (500 MHz, DMSO-d_6) δ 10.83 (d, J = 13.6 Hz, 1H), 8.42 (d, J = 13.1 Hz, 1H), 7.65 (s, 1H), 7.56–7.61 (m, 1H), 7.25 (d, J = 8.3 Hz, 1H), 4.20 (q, J = 7.3 Hz, 2H), 4.11 (q, J = 7.3 Hz, 2H), 2.25 (s, 3H), 1.24 (td, J = 6.9, 10.5 Hz, 6H). LCMS found 404.16 $[M+H]^+$. Then to the diethyl 2-((4-iodo-2-methylphenylamino)methylene)malonate (9.0 g, 22.3 mmol) was added diphenyl ether (35.5 mL,

223 mmol). The reaction was run for 45 min at 250 °C. The mixture was cooled, and isohexane was added (30 mL). The solid formed (light yellow solid) was collected by filtration and washed further with isohexane (30 mL). The solid was dried under high vacuum to give the desired product as a light yellow solid (Yield: 100%). ^{1}H NMR (400 MHz, DMSO-d_6) δ 11.74 (br. s., 1H), 8.37 (s, 1H), 8.28 (s, 1H), 7.89 (s, 1H), 4.21 (q, J = 7.3 Hz, 2H), 1.26 (t, J = 7.3 Hz, 3H). LCMS found 357.95 $[M+H]^+$.

4-chloro-6-iodo-8-methylquinoline-3-carboxamide (7)

NaOH (1.96 g, 49.1 mmol) was dissolved in water (40 mL) and ethanol (20 mL). The resultant solution was added to **6** (7.97 g, 22.32 mmol), and the mixture was heated and refluxed for 1 h with stirring. Then concentrated HCl was added until a white precipitate formed. The reaction was stirred overnight at room temperature. After stirring overnight, the precipitate was filtered, washed with water and dried in vacuo to give 6-iodo-8-methyl-4-oxo-1,4-dihydroquinoline-3-carboxylic acid as a white solid. (LCMS found 329.89 $[M+H]^+$). To 6-iodo-8-methyl-4-oxo-1,4-dihydroquinoline-3-carboxylic acid (7.34 g, 22.30 mmol) was added thionyl chloride (24.42 mL, 335 mmol), then three drops DMF were added. The mixture was refluxed for 2 h. The excess thionyl chloride was evaporated in vacuo, and the residue was azeotroped with toluene (5 mL, 1×). The crude product 4-chloro-6-iodo-8-methylquinoline-3-carbonyl chloride was used in the next step without further characterization. To stirred ammonium hydroxide (34.7 mL, 892 mmol) was added portionwise 4-chloro-6-iodo-8-methylquinoline-3-carbonyl chloride (8.16 g, 22.3 mmol), and the mixture was stirred at room temperature overnight. The solid formed was filtered, washed with water, and dried under vacuum at 60 °C to give **7** as a white solid (Yield: 80%). ^{1}H NMR (400 MHz, DMSO-d_6) δ 8.89 (s, 1H), 8.46 (s, 1H), 8.20 (br. s., 1H), 8.10 (s, 1H), 7.99 (br. s., 1H), 2.70 (s, 3H). LCMS found 346.87 $[M+H]^+$.

6-iodo-4-(3-methoxyphenylamino)-8-methylquinoline-3-carboxamide (8)

Compound **7** (174 mg, 0.499 mmol) was dissolved in acetonitrile, and 3-methoxyaniline (0.059 mL, 0.52 mmol) was added. The mixture was heated and refluxed overnight. The precipitate formed was filtered, washed with acetonitrile, and the solid (light yellow solid) obtained was dried under high vacuum to give the title compound (Yield: 90%). ^{1}H NMR (400 MHz, DMSO-d_6) δ 8.78 (s, 1H), 8.39 (br. s., 1H), 8.31 (br. s., 1H), 8.10 (br. s., 1H), 7.74 (br. s., 1H), 7.28 (t, J = 8.0 Hz, 1H), 6.73–6.86 (m, 3H), 3.72 (s, 3H), 2.65 (s, 3H). LCMS found 434.97 $[M+H]^+$.

Methyl 3-(3-carbamoyl-4-(3-methoxyphenylamino)-8-methylquinolin-6-ylthio)benzoate (9a)

To **8** (20.0 mg, 0.046 mmol) was added $Pd_2(dba)_3$ (8.4 mg, 9.23 μmol), then 2,2′-oxybis(2,1-phenylene)bis(diphenylphosphine) (9.9 mg, 0.018 mmol). The methyl 3-mercaptobenzoate (11.6 mg, 0.069 mmol) was dissolved in toluene (1.5 mL) and then added to the solids. Lastly, KOtBu (0.092 mL, 0.092 mmol) was added. The mixture was placed in the MW and heated for 40 min at 170 °C. The crude product was filtered through Celite after adding methanol and further washed with methanol. The solvent was concentrated. The crude product was chromatographed using 50–100% EtOAC in hexane to give the desired product **9a** as an orange solid (Yield: 75%). ^{1}H NMR (400 MHz, CD_3OD) δ 8.91 (s, 1H), 7.91 (d, J = 7.3 Hz, 1H), 7.85 (s, 1H), 7.50 (s, 1H), 7.42–7.46 (m, 2H), 7.33–7.40 (m, 1H), 6.99 (t, J = 8.0 Hz, 1H), 6.49–6.53 (m, 1H), 6.30–6.36 (m, 2H), 3.91 (s, 3H), 3.66 (s, 3H), 2.69 (s, 3H). LCMS found 474.01, $[M+H]^+$.

4-((3-methoxyphenyl)amino)-8-methyl-6-(phenylthio)quinoline-3-carboxamide (9b)

To compound **8** (40.0 mg, 0.092 mmol) were added $Pd_2(dba)_3$ (16.9 mg, 0.018 mmol) and 2,2′-oxybis(2,1-phenylene)bis(diphenylphosphine) (19.9 mg, 0.037 mmol). The benzenethiol (0.014 mL, 0.138 mmol) was dissolved in toluene and added to the solids. Lastly, KOtBu (0.115 mL, 0.185 mmol) was added. The mixture was heated in the MW for 40 min at 170 °C. To the crude product was added methanol, and the solution was filtered through Celite. Then, the solvent was concentrated. The crude product was chromatographed 0–100% EtOAc in hexane to give the desired product as a yellow solid. (Yield: 53%). ^{1}H NMR (400 MHz, CD_3OD) δ 8.89 (s, 1H), 7.44 (s, 2H), 7.18–7.29 (m, 5H), 7.08 (t, J = 8.0 Hz, 1H), 6.58–6.64 (m, 1H), 6.34–6.40 (m, 2H), 3.71 (s, 3H), 2.67 (s, 3H). LCMS found 416.01, $[M+H]^+$.

Methyl 3-(3-carbamoyl-4-(3-methoxyphenylamino)-8-methylquinolin-6-ylsulfonyl)benzoate (10a)

To **9a** (103 mg, 0.218 mmol) was added oxone (401 mg, 0.653 mmol) in DMF (5 mL). The reaction was stirred at room temperature for 5 h. Then, the reaction mixture was poured into water (40 mL) and extracted with DCM (5×), and the combined organic layers were dried (Na_2SO_4) and concentrated. The crude product was chromatographed using 0–10% MeOH in DCM to give the desired product as an orange solid (Yield: 85%). ^{1}H NMR (500 MHz, $CDCl_3$) δ 10.86 (s, 1H), 8.93 (s, 1H), 8.44 (s, 1H), 8.23–8.26 (m, 1H), 8.21 (d, J = 7.8 Hz, 1H), 7.91 (s, 1H), 7.77 (d, J = 7.8 Hz, 1H), 7.54 (t, J = 7.8 Hz, 1H), 7.15 (t, J = 8.0 Hz, 1H), 6.75 (dd, J = 1.95, 8.3 Hz, 1H), 6.57 (d, J = 7.8 Hz, 1H), 6.54 (s, 1H), 5.90–6.10 (br. s.,2H), 3.97 (s, 3H), 3.65 (s, 3H), 2.75 (s, 3H). LCMS found 506.01, $[M+H]^+$.

4-((3-methoxyphenyl)amino)-8-methyl-6-(phenylsulfonyl)quinoline-3-carboxamide (10b)

To compound **9b** (13.4 mg, 0.032 mmol) were added oxone (59.5 mg, 0.097 mmol) and DMF (3 mL). The reaction

was stirred for 4 h at rt. Then, the reaction mixture was poured into water (20 mL) and extracted with DCM (5×), the combined organics were washed with brine (1×) and dried under sodium sulfate. The crude product was chromatographed using 50–70% EtOAc in hexane to give the desired product as a light yellow solid. (Yield: 62%).^{1}H NMR (400 MHz, CD_3OD) δ 9.03 (s, 1H), 8.38 (s, 1H), 7.93 (s, 1H), 7.72 (d, J = 7.3 Hz, 2H), 7.64 (t, J = 7.3 Hz, 1H), 7.55 (t, J = 7.7 Hz, 2H), 7.24 (t, J = 8.0 Hz, 1H), 6.82 (dd, J = 1.8, 8.4 Hz, 1H), 6.63 (d, J = 7.3 Hz, 1H), 6.57 (s, 1H), 3.64 (s, 3H), 2.74 (s, 3H). LCMS found 448.01, $[M+H]^+$.

3-(3-carbamoyl-4-(3-methoxyphenylamino)-8-methylquinolin-6-ylsulfonyl)benzoic acid (11)

A solution of **10a** (60.0 mg, 0.119 mmol) in ethanol (2 mL) was treated with NaOH (0.890 mL, 1.780 mmol), and the resulting solution was stirred at 45 °C overnight. The solvent was evaporated. The residue was dissolved in water and acidified with 1 M HCl to pH 4. The resulting precipitate was filtered, washed with water, and dried in vacuo. The crude product was purified via preparative HPLC to give the desired product as a yellow solid (Yield: 31%). ^{1}H NMR (400 MHz, CD_3OD) δ 9.01 (s, 1H), 8.38 (s, 1H), 8.34 (s, 1H), 8.24 (d, J = 7.3 Hz, 1H), 7.99 (s, 1H), 7.86 (d, J = 8.0 Hz, 1H), 7.65 (t, J = 7.7 Hz, 1H), 7.18 (t, J = 8.0 Hz, 1H), 6.74–6.79 (m, 1H), 6.53–6.62 (m, 2H), 3.62 (s, 3H), 2.75 (s, 3H). LCMS found 492.01, $[M+H]^+$.

6-(3-carbamoylphenylsulfonyl)-4-(3-methoxyphenylamino)-8-methylquinoline-3-carboxamide (12a)

A solution of **10a** (18.0 mg, 0.036 mmol) in dioxane was added to a solution of ammonium hydroxide (0.761 mL, 19.55 mmol). The mixture was stirred at room temperature overnight. Then the solvent was concentrated, and the residue was partitioned between sat. NH_4Cl and ethyl acetate. The aqueous layer was extracted with EtOAc (3×), and the combined organics were washed with brine and dried over Na_2SO_4. After filtration and evaporation, the crude product was chromatographed using 0–10% MeOH to give the desired product as a yellow solid (Yield: 18%). ^{1}H NMR (400 MHz, CD_3OD) δ 9.02 (s, 1H), 8.36 (s, 1H), 8.31 (s, 1H), 8.10 (s, 1H), 7.99 (s, 1H), 7.81 (d, J = 7.3 Hz, 1H), 7.65 (t, J = 8.0 Hz, 1H), 7.17 (t, J = 8.4 Hz, 1H), 6.75–6.80 (m, 1H), 6.55–6.60 (m, 2H), 3.64 (s, 3H), 2.75 (s, 3H). LCMS found 491.01, $[M+H]^+$.

4-(3-methoxyphenylamino)-8-methyl-6-(3-(methylcarbamoyl)phenylsulfonyl)quinoline-3-carboxamide (12b)

To **11** (8.6 mg, 0.017 mmol) in DMF was added HATU (7.3 mg, 0.019 mmol). After 5 min, methylamine HCl (1.14 mg, 0.017 mmol) and DIEA (6.4 μL, 0.037 mmol) were added. The resulting solution was stirred at room temperature for 6 h. The solvent was concentrated. The crude product was purified via preparative HPLC to give the desired product as a yellow solid (Yield: 37%). ^{1}H NMR (400 MHz, DMSO-d_6) δ 10.77 (s, 1H), 9.08 (s, 1H), 8.71 (d, J = 4.4 Hz, 1H), 8.32–8.35 (m, 1H), 8.29 (br. s., 1H), 8.26 (s, 1H), 8.08 (d, J = 8.0 Hz, 1H), 7.99 (s, 1H), 7.76 (d, J = 7.3 Hz, 2H), 7.68 (t, J = 7.7 Hz, 1H), 7.12 (t, J = 8.0 Hz, 1H), 6.69 (dd, J = 1.8, 8.4 Hz, 1H), 6.60 (s, 1H), 6.52 (d, J = 7.3 Hz, 1H), 3.62 (s, 3H), 2.81 (d, J = 4.4 Hz, 3H), 2.69 (s, 3H). LCMS found 505.01, $[M+H]^+$.

Methyl 3-(3-carbamoyl-4-(3-methoxyphenylamino)-8-methylquinolin-6-ylamino)benzoate (13)

To **8** (40.0 mg, 0.092 mmol) was added 2,2′-oxybis(2,1-phenylene)bis (diphenylphosphine) (19.9 mg, 0.037 mmol), then Pd(dppf)Cl_2·DCM (13.5 mg, 0.018 mmol) and methyl 3-aminobenzoate (27.9 mg, 0.185 mmol). Lastly, KOtBu (0.185 mL, 0.185 mmol) was added. The reaction mixture was heated in the MW for 20 min at 160 °C. After the reaction mixture cooled to ambient temperature, the crude was filtered through Celite washing with MeOH (3×). The solvent was concentrated under reduced pressure. Then, the crude product was purified via preparative HPLC to give **13** as a yellow solid (Yield: 12%). ^{1}H NMR (400 MHz, CD_3OD) δ 8.76 (s, 1H), 7.55 (s, 1H), 7.46 (d, J = 8.0 Hz, 1H), 7.30 (d, J = 2.9 Hz, 1H), 7.26 (s, 1H), 7.13 (t, J = 8.0 Hz, 1H), 7.08 (t, J = 8.0 Hz, 1H), 6.95 (dd, J = 1.5, 8.0 Hz, 1H), 6.62 (dd, J = 1.8, 8.4 Hz, 1H), 6.50 (t, J = 2.2 Hz, 1H), 6.43–6.47 (m, 1H), 3.88 (s, 3H), 3.70 (s, 3H), 2.70 (s, 3H). LCMS found 457.01, $[M+H]^+$.

8-ethyl-6-iodo-4-((3-methoxyphenyl)amino) quinoline-3-carboxamide (16b)

To **15b** (19,20) (302 mg, 0.838 mmol) were added acetonitrile and 3-methoxyaniline (0.099 mL, 0.879 mmol). The mixture was heated at 80 °C overnight. Then the solvent was concentrated, and the crude product was purified via chromatography (0–6% MeOH in DCM) to give **16b** as a light yellow solid (Yield: 78%). LCMS found 447.99 $[M+H]^+$. The product was taken to the next step without further characterization.

General procedure A. Synthesis of intermediate **23** was achieved via published methods (16,19,20) and is summarized in the Supporting Information (Appendix S1). For example, compound **7** was dissolved in acetonitrile, and the desired amine (1.1 equiv) was added. The mixture was generally heated under reflux overnight or run in the microwave at 145 °C for 25 min unless stated otherwise in the protocol. Then the precipitate formed was filtered, washed with acetonitrile, and the solid obtained was dried under high vacuum to give **23**. These analogs were confirmed by LCMS and/or NMR and used in the next step (General procedure B) without further characterization.

General procedure B. Suzuki coupling protocol. To iodo-substituted templates 8 and 23 **-** (1 equiv.) were

added the desired boronic acid or ester (1.5 equiv.), Pd(dppf)Cl_2·DCM (0.1 equiv.), dioxane, and sodium carbonate (6 equiv.). The reaction mixture was heated in the MW at 130 °C, 145 °C, or 160 °C as specified in Scheme 2 or Scheme 3 for 20 min. After the reaction mixture cooled to ambient temperature, the crude was filtered through Celite washing with MeOH/DCM (1:9). The filtrate was concentrated under reduced pressure. Unless otherwise noted, the crude products were chromatographed or purified via preparative HPLC to give the desired products of the general templates **17, 19, 22e,f, and 24**, which are characterized in the Supporting Information (Appendix S1).

General procedure C. To **20** (1 equiv.) was added acetonitrile, and the required amine (5–6 equiv.) was added. The reaction was run at 80 °C in a sealed vial for 48 h. The solvent was concentrated, and the crude product was purified via preparative HPLC or chromatography to afford the products (**22a-d**), which are characterized in the Supporting Information (Appendix S1).

5-(3-carbamoyl-4-((3-methoxyphenyl)amino)-8-methylquinolin-6-yl)isophthalic acid (18a)

To **17e** (7.00 mg, 0.014 mmol) was added LiOH (2.014 mg, 0.084 mmol), and the solids were dissolved in a mixture of water:THF:MeOH (1:1:1). The solution was stirred at 90 °C in a sealed vial for 2 h. Then the solvent was concentrated. The crude product was purified via PREP HPLC to give 5-(3-carbamoyl-4-((3-methoxyphenyl) amino)-8-methylquinolin-6-yl)isophthalic acid (**18a**), (white solid, Yield: 25%). ^{1}H NMR (500 MHz, DMSO-d_6) δ 13.25 (br. s., 1H), 10.47 (s, 1H), 8.99 (s, 1H), 8.39 (s, 1H), 8.21 (s, 1H), 8.15 (m, 2H), 7.96 (s, 2H), 7.67 (s, 1H), 7.15 (t, J = 8.0 Hz, 1H), 6.62–6.56 (m, 2H), 6.54 (d, J = 7.0 Hz, 1H), 3.68 (s, 3H), 2.77 (s, 3H). LCMS found 472.01, $[M+H]^+$.

3-(3-carbamoyl-4-((3-methoxyphenyl)amino)-8-methylquinolin-6-yl)-5-(methoxycarbonyl)benzoic acid (18b)

To **17e** (11.40 mg, 0.023 mmol) was added LiOH (0.273 mg, 0.011 mmol), and the solids were dissolved in a mixture of water:THF:MeOH (1:1:1). The reaction mixture was stirred at rt for 12 h. Then another 0.5 equiv. of LiOH was added, and the temperature was raised to 50 °C. The reaction ran 6 more hours at 50 °C, and then the solvent was concentrated. The crude product containing the diester and the monoacid was chromatographed (0–10% MeOH/DCM) to give 3-(3-carbamoyl-4-((3-methoxyphenyl) amino)-8-methylquinolin-6-yl)-5-(methoxycarbonyl) benzoic acid (**18b**), (white solid, Yield: 12%). ^{1}H NMR (500 MHz, DMSO-d_6) δ 10.50 (s, 1H), 9.00 (s, 1H), 8.42 (s, 1H), 8.24 (d, J = 7.3 Hz, 2H), 8.04 (br. s., 1H), 7.95 (s, 2H), 7.69 (br. s., 1H), 7.17 (t, J = 8.0 Hz, 1H), 6.66 (dd, J = 1.9, 8.3 Hz, 1H), 6.62 (s, 1H), 6.55 (d, J = 7.8 Hz, 1H), 3.90 (s, 3H), 3.68 (s, 3H), 2.77 (s, 3H). LCMS found 486.01, $[M+H]^+$.

Methyl 3-(3-carbamoyl-4-chloro-8-methylquinolin-6-yl)benzoate (20a), dimethyl 3,3′-(3-carbamoyl-8-methylquinoline-4,6-diyl)dibenzoate (21a), and methyl 3-(3-carbamoyl-8-methylquinolin-6-yl) benzoate (21b)

To **7** (200 mg, 0.577 mmol) were added (3-(methoxycarbonyl)phenyl)boronic acid (104 mg, 0.577 mmol), Pd(dppf)Cl_2·DCM (84 mg, 0.115 mmol), dioxane (4 mL), and sodium carbonate (1.73 mL, 3.46 mmol). The reaction mixture was heated in the MW at 150 °C for 10 min. After the reaction mixture cooled to ambient temperature, the crude was filtered through Celite washing with MeOH/DCM (1:9). The filtrate was concentrated under reduced pressure. The crude mixture was chromatographed using hexanes/EtOAc to give as the major product **20** as a white solid (Yield: 29%) and a mixture of **21a** and **21b**. This mixture was separated using preparative HPLC to give the clean products **21a** (white solid, Yield: 5%) and **21b** (white solid, Yield: 2%). (**20**). ^{1}H NMR (500 MHz, DMSO-d_6) δ 8.90 (s, 1H), 8.30–8.35 (m, 2H), 8.21 (s, 1H), 8.13–8.17 (m, 2H), 8.03 (d, J = 7.8 Hz, 1H), 7.99 (s, 1H), 7.70 (t, J = 7.8 Hz, 1H), 3.91 (s, 3H), 2.82 (s, 3H). LCMS found 354.01, $[M+H]^+$. (**21a**). ^{1}H NMR (500 MHz, DMSO-d_6) δ 9.00 (s, 1H), 8.07–8.12 (m, 3H), 7.99 (s, 1H), 7.95 (d, J = 7.8 Hz, 1H), 7.83–7.89 (m, 2H), 7.69–7.75 (m, 2H), 7.60 (t, J = 7.8 Hz, 1H), 7.54 (s, 1H), 7.48–7.50 (m, 1H), 3.32 (s, 6H), 2.87 (s, 3H). LCMS found 455.11, $[M+H]^+$. (**21b**). ^{1}H NMR (500 MHz, $CDCl_3$) δ 9.31 (s, 1H), 8.69 (d, J = 2.4 Hz, 1H), 8.40 (s, 1H), 8.09 (d, J = 7.8 Hz, 1H), 7.97 (d, J = 7.3 Hz, 2H), 7.91 (d, J = 7.8 Hz, 1H), 7.59 (t, J = 7.5 Hz, 1H), 3.98 (s, 3H), 2.91 (s, 3H). LCMS found 321.01, $[M+H]^+$.

4-chloro-6-iodo-N,8-dimethylquinoline-3-carboxamide (25a)

To sodium hydride (60 % dispersion in mineral oil, 10.9 mg, 0.27 mmol) in DMF (2 mL) was added intermediate **7** (100 mg, 0.289 mmol) in dry DMF (3 mL). The reaction mixture was stirred for 35 min at rt before adding iodomethane (0.017 mL, 0.274 mmol), after which the reaction mixture was stirred at rt overnight. Water and EtOAc were added, and the aqueous layer was extracted with EtOAc (3×). The combined organics were washed with brine and finally dried under sodium sulfate. The solvent was concentrated, and the product was confirmed by LCMS, LCMS found 360.01, $[M+H]^+$. The product was taken to the next step without further characterization.

4-chloro-6-iodo-N,N,8-trimethylquinoline-3-carboxamide (25b)

To sodium hydride (60 % dispersion in mineral oil, 23 mg, 0.57 mmol) in DMF (2 mL) was added intermediate **7** (100 mg, 0.289 mmol) in dry DMF (3 mL). The reaction mixture was stirred for 35 min at rt before adding iodomethane (0.020 mL, 0.317 mmol), after which the reaction mixture was stirred at rt overnight. Then, to the reaction mixture were added water and EtOAc. The aqueous layer

was extracted with EtOAc (3×). The combined organics were washed with brine and finally dried under sodium sulfate. The solvent was concentrated, and the product was confirmed by LCMS, LCMS found 374.01, $[M+H]^+$. The product was taken to the next step without further characterization.

6-iodo-4-((3-methoxyphenyl)amino)-N,8-dimethylquinoline-3-carboxamide (26a)

To **25a** (104 mg, 0.288 mmol) were added acetonitrile and 3-methoxyaniline (0.034 ml, 0.303 mmol). The mixture was heated under reflux overnight. The solution was filtered, and the solids were washed with acetonitrile. The filtrate was concentrated. The product **26a** (Yield: 41%) was confirmed by LCMS (found 448.04 $[M+H]^+$) and was taken to the next step without further characterization.

6-iodo-4-((3-methoxyphenyl)amino)-N,N,8-trimethylquinoline-3-carboxamide (26b)

To **25b** (56.0 mg, 0.149 mmol) were added acetonitrile and 3-methoxyaniline (0.018 ml, 0.157 mmol). The mixture was heated under reflux overnight. The solution was filtered, and the solids were washed with acetonitrile. The filtrate was concentrated. The product (Yield: 61%) was confirmed by LCMS (462.01, $[M+H]^+$) and was taken to the next step without further characterization.

4-((3-methoxyphenyl)amino)-N,8-dimethyl-6-(1-methyl-1H-indazol-6-yl)quinoline-3-carboxamide (27a) (synthesized using General procedure B from 26a, yellow solid, Yield: 8%)

^{1}H NMR (500 MHz, DMSO-d_6) δ 10.05 (s, 1H), 8.87 (s, 1H), 8.59 (d, J = 4.4 Hz, 1H), 8.14 (s, 1H), 8.07 (s, 1H), 8.06 (s, 1H), 7.80 (d, J = 8.3 Hz, 1H), 7.69 (s, 1H), 7.34–7.37 (m, 1H), 7.21 (t, J = 8.0 Hz, 1H), 6.64–6.68 (m, 2H), 6.58 (d, J = 8.3 Hz, 1H), 4.07 (s, 3H), 3.70 (s, 3H), 2.80 (s, 3H), 2.66 (d, J = 4.4 Hz, 3H). LCMS found 452.01, $[M+H]^+$.

4-((3-methoxyphenyl)amino)-N,N,8-trimethyl-6-(1-methyl-1H-indazol-6-yl)quinoline-3-carboxamide, formic acid salt (27b), (synthesized using General procedure B from 26b, yellow solid, Yield: 17%)

^{1}H NMR (500 MHz, DMSO-d_6) δ 9.11 (s, 1H), 8.55 (s, 1H), 8.51 (s, 1H), 8.13 (s, 2H), 8.07 (s, 1H), 8.04 (s, 1H), 7.86 (d, J = 8.3 Hz, 1H), 7.66 (d, J = 8.3 Hz, 1H), 7.17 (t, J = 8.5 Hz, 1H), 6.63 (d, J = 8.3 Hz, 1H), 6.55–6.59 (m, 2H), 4.12 (s, 3H), 3.71 (s, 3H), 2.79 (s, 3H), 2.75 (s, 3H), 2.38 (s, 3H). LCMS found 466.01, $[M+H]^+$.

4-(cyclopentylamino)-8-methyl-6-(3-(oxazol-2-yl)phenyl)quinoline-3-carboxamide (28)

To **20b** (13.00 mg, 0.036 mmol) were added acetonitrile and lastly cyclopentanamine (0.021 mL, 0.214 mmol). The reaction was run at 80 °C in a sealed vial for 48 h. The solvent was concentrated, and the crude product was chromatographed using 0–7% MeOH in DCM to give the desired product as a yellow solid (Yield: 34%).^{1}H NMR (500 MHz, $CDCl_3$) δ 9.50 (d, J = 7.3 Hz, 1H), 8.75 (s, 1H), 8.39 (d, J = 4.8 Hz, 2H), 8.07 (d, J = 7.8 Hz, 1H), 7.87 (s, 1H), 7.76 (s, 1H), 7.75 (d, J = 7.8 Hz, 1H), 7.59 (t, J = 7.6 Hz, 1H), 7.29 (s, 1H), 5.90 (br. s., 2H), 4.55–4.64 (m, 1H), 2.80 (s, 3H), 2.11–2.20 (m, 2H), 1.78–1.90 (m, 4H), 1.68–1.75 (m, 2H). LCMS found 413.01, $[M+H]^+$.

Molecular modeling

Docking for all compounds was performed using POSIT v 1.0.2 (OpenEye Scientific Software: Santa Fe, NM, USA). The co-ordinates of the *apo* crystal structure of TbrPDEB1 were downloaded from the Protein Data Bank (PDB), PDB code: 4I15 (21). The protein was prepared for docking, and mild ligand–protein clashes were allowed to account for the average co-ordinate error expected in PDB structures. The 'combine-receptors' option was used to include the binding mode observed in the human phosphodiesterase 4B2B in complex with a quinoline Inhibitor during docking in TbrPDEB1 (PDB code: 3FRG) (19). Mild clashes were also used in pose prediction. All the other options in POSIT were kept as default. The docked poses were energy minimized using SZYBKI (v 1.7.0 OpenEye Scientific Software) allowing partial relaxation of the protein residues in the direct proximity to the ligand. The docking program FRED v 3.0.0 (OpenEye Scientific Software) was also used to investigate alternative binding modes (such as for compound **28**).

Water molecule predictions were performed using SZMAP v 1.1.0 (OpenEye Scientific Software) on three different protein–ligand complex structures: (i) the crystal structure of the human phosphodiesterase 4B2B(15), (ii) the TbrPDEB1–**19a** complex, and (iii) the TbrPDEB1–**24g** complex. The conformations of the ligands of the two latter protein–ligand complexes were obtained with molecular docking. The protein–ligand complexes were used as input to SZMAP, which was then used to predict the solvation of the active binding site in complex with the ligands using the semi-continuum solvation theory, in combination with a single explicit water probe. The results were visualized with VIDA (OpenEye Scientific Software).

Results

In the interest of exploring the SAR around **3**, we divided the compound into 4 regions, highlighted in Figure 1. First, we synthesized a set of analogs to determine the preferred aryl substituent and connection to the quinoline core for Region A, following Scheme 1. Synthesis commenced with the condensation of **5a** with diethyl ethoxymethylenemalonate, followed by cyclization to afford **6**. The ester was hydrolyzed to the acid, and the resulting product was

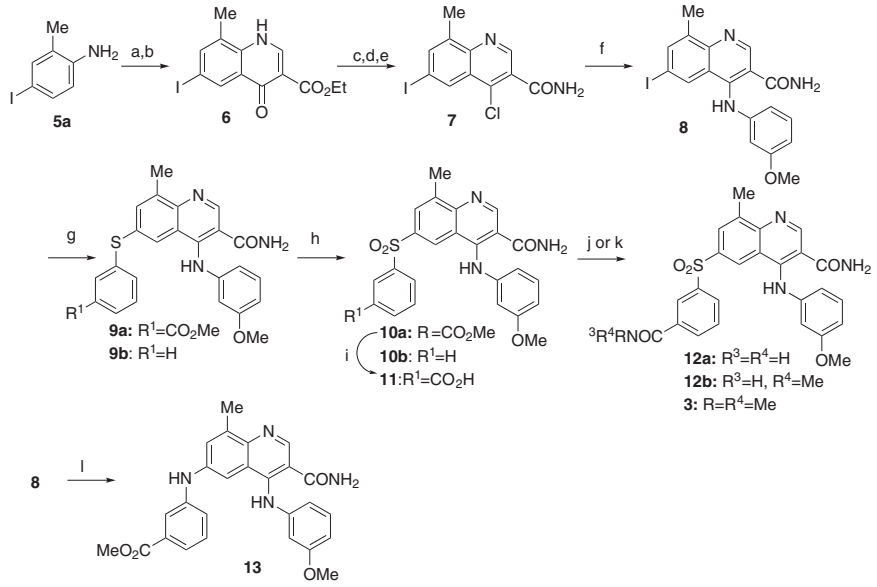

Scheme 1: Preparation of analog **13**, exploring Region A (Reagents and conditions**.** (a) $EtOCH{=}C(CO_2Et)_2$, 100 °C, 1 h (98%). (b) Ph_2O, 250 °C, 45 min (100%). (c) NaOH, EtOH, reflux, 1 h, then conc. HCl, overnight. (d) $SOCl_2$, DMF, 80 °C, 2 h. (e) NH_4OH, rt, overnight (80%). (f) 3-methoxyaniline, MeCN, 80 °C, overnight (90%). (g) 3-substituted (R^1) benzenethiols, $Pd_2(dba)_3$, DPEphos, KOtBu, toluene, 170 °C, MW, 30 min (70–85%). (h) Oxone, DMF, rt, 12–24 h (70–90%). (i) NaOH, EtOH, 45°C, overnight (31%). (j) **11**, Me_2NH or $MeNH_2{\cdot}HCl$, HATU, DIEA, DMF, rt (for **3** (21%) and **12b** (37%). (k) for **10a**: NH_4OH, dioxane, rt, overnight (12a,18%). (l) methyl 3-aminobenzoate, $Pd(dppf)Cl_2$, (oxybis(2,1-phenylene))bis (diphenylphosphine), KOtBu, dioxane, 160 °C, MW, 20 min (12%)).

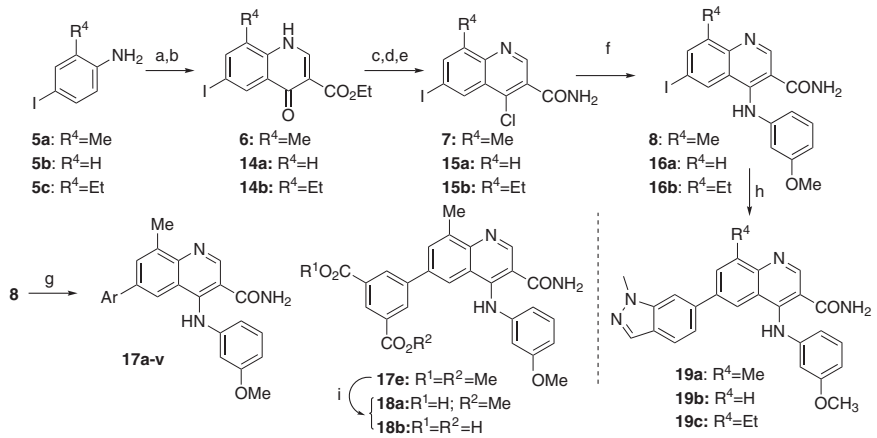

Scheme 2: Preparation of analogs **17-19** (Reagents and conditions. (a) $EtOCH{=}C(CO_2Et)_2$, 100 °C, 1 h (80–98%). (b) Ph_2O, 250 °C, 45 min (81–100%). (c) NaOH, EtOH, reflux, 1 h, then conc. HCl, overnight. (d) $SOCl_2$, DMF, 80 °C, 2 h. (e) NH_4OH, rt, overnight (61–92%). (f) 3-methoxyaniline, MeCN, 80 °C, overnight (78–94%). (g) Ar-$B(OH)_2$, Na_2CO_3, $Pd(dppf)Cl_2$, dioxane, 130 or 145 °C, MW, 20 min (20–70%). (h) 1-Methyl-1*H*-indazole-6-boronic acid, Na_2CO_3, $Pd(dppf)Cl_2$, dioxane, 160 °C, MW, 20 min (13–56%). (i) LiOH, H_2O:THF: MeOH, rt, 12 h).

chlorinated and quenched with aqueous ammonia affording the primary carboxamide **7**. Reaction of **7** with *m*-anisidine under reflux provided **8** in high yield. This template was reacted with commercially available aryl thiols using palladium catalysis to provide the sulfides, **9**, which could be oxidized to the appropriate sulfones **10** using Oxone.

Amide substituents were introduced via hydrolysis of the ester functionality of **10a** under basic conditions to give **11**, and then standard amide coupling with the appropriate amine provided **3** and **12b**. Treatment of **10a** with ammonium hydroxide gave analog **12a**. To explore a nitrogen linker to Region A, the reaction of the commercial methyl 3-aminobenzoate with **8** using a modified palladium-catalyzed coupling procedure provided **13** (22,23).

Following synthesis, the analogs were tested at a single concentration (10 μM) against TbrPDEB1, and those

Table 1: Biochemical potency data for analogs of **3**[a]

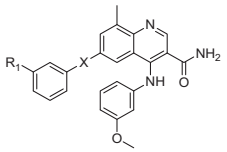

Compound	R_1	X	TbrPDEB1 (% inh)	TbrPDEB1 (IC_{50} μM)	TbrPDEB2 (IC_{50} μM)
3	$CONMe_2$	SO_2	51 ± 3.9	24 ± 1.7	29.8 ± 7.5
9a	CO_2Me	S	12 ± 6.1	–	–
9b	H	S	10.0[b]		
10a	CO_2Me	SO_2	70 ± 7.9	3.5 ± 0.3	15.1 ± 3.9
10b	H	SO_2	21 ± 16	–	–
11	CO_2H	SO_2	82 ± 10	2.9 ± 0.8	6.8 ± 0.6
12a	$CONH_2$	SO_2	64 ± 7	–	–
12b	CONHMe	SO_2	66 ± 6.1	31 ± 5.8	–
13	CO_2Me	NH	84 ± 7.7	16 ± 1.7	–

[a]All values are the mean of three or more replicates ± SEM.
[b]n = 1.

compounds with >65% inhibition, and those that represented key SAR points, were tested in a dose–response assay. We noted that removal of N-alkyl groups from the benzamide of **3** results in little change in percentage inhibition, the key data in selecting compounds for IC_{50} determination (**3**, **12a-b**, Table 1). Replacement of the carboxamide with an ester (**10a**) or carboxylic acid (**11**) improved activity by approximately 8-fold over **3**. The sulfone linker between the quinoline and side chain was better than either a sulfide (**9a**) or amine (**13**).

Having explored the sulfone, sulfide, and amine linker of the A region of the inhibitor, we designed analogs with no intervening atom between the core template and the A region via a biaryl linkage. This was accomplished using the route shown in Scheme 2. The iodo template **16** was prepared using a route analogous to the preparation of **8**, followed by reaction with various boronic acids using Suzuki coupling chemistry.

The potency of the biaryl analog **17a** on TbrPDEB1 (Table 2) was within twofold of the IC_{50} of the matched sulfone analog **10a** (Table 1). The observation that the matched biaryl linker was essentially equivalent to the more synthetically intensive sulfone linker allowed us to access a larger set of analogs via one-step synthesis from the iodo template (8 or 16) and boronates using Suzuki couplings. We explored the SAR for this region with the biaryl linkage using various aryl boronic acids or esters obtained from commercial sources, or via synthesis (Appendix S1, Supporting Information) (24–26). Besides close-in analogs of **17a**, we explored small, heterocyclic replacements and bioisosteres for the methyl ester moiety (Table 2, **17o-17r**). A small set of analogs bearing fused bicyclic heteroaromatic rings was also prepared (**17t-v**, **19a**). Notably, the potency of the N-methyl indazole analog **19a** was within twofold of the potency of **17a**. Additionally, the hydrolysis of the diester groups of **17e** provided the mono- and diacids **18a-b**, which showed low (<50%) inhibition at 10 μM.

The 3-methyl ester substitution was preferred over the 2 or 4 position (Table 2, **17a-17c**). We noted that several compounds bearing replacements for the methyl ester of **17a** (**17m**, **17o**, **17p, 17t**) were approximately equipotent, although none was significantly better. Given their increase in complexity and size over **17a**, these analogs were less desirable. The tetrazole analog **17m** was more potent than the corresponding bioisosteric carboxylic acid (**17d**), which was not potent enough to advance to IC_{50} determination.

The potency of the best biaryl compound in Table 2 (**19a**) is similar to the best sulfone from Table 1 (**11**), leading us to focus upon these biaryl compounds given their ease of synthesis and purification compared to the sulfone analogs. With this in mind, we next turned our attention to preparation of Region B variants, keeping Region A constant with either of the two best Region A substituents: the methyl indazole fragment of **19a** or the methylbenzoate fragment of **17a**.

These analog syntheses were accomplished using one of the two routes shown in Scheme 3. Reaction of **7** with (3-(methoxycarbonyl)phenyl)boronic acid using Suzuki coupling afforded **20**, the bis-arylated product **21,** and the dehalogenated byproduct **21b**. The final step required heating of **20** with the desired amine to give **22a-d,** and **28**. Additionally, reaction of **7** with various amines under reflux provided intermediates **23** (General procedure A and Appendix S1, Supporting Information), followed by reaction of these intermediates *via* Suzuki coupling with 1-methyl-1H-indazol-6-ylboronic acid to give **24a-g** or 3-(methoxycarbonyl)phenylboronic acid to afford **22e-f**.

Table 2: Analogs exploring the Region A of **3**[a]

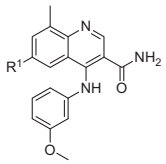

Compound	R^1	TbrPDEB1 (% inh)	TbrPDEB1 (IC_{50} μM)	TbrPDEB2 (IC_{50} μM)
17a	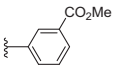	94 ± 3.5	6.4 ± 1.7	6.2 ± 0.6
17b		37 ± 14		
17c	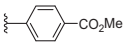	6 ± 1.4	–	
17d	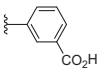	54 ± 8.8	–	
17e	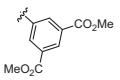	50 ± 6.1	–	
17f	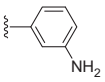	35 ± 10	23 ± 4.0	
17g	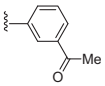	65 ± 5.5	nd[b]	
17h		9 ± 7.1	–	
17i	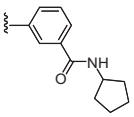	8.6 ± 5.2	–	
17j	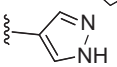	74 ± 13	9 ± 0.6	
17k	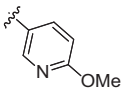	10 ± 6.9	–	
17l		43 ± 16	–	
17m	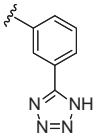	83 ± 7.5	6.7 ± 2.9	4.6 ± 0.1
17n	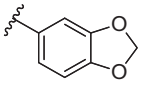	13 ± 8	–	

Table 2: continued

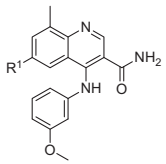

Compound	R^1	TbrPDEB1 (% inh)	TbrPDEB1 (IC_{50} μM)	TbrPDEB2 (IC_{50} μM)
17o	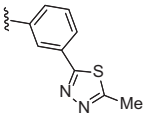	83 ± 1.3	6 ± 1.7	
17p	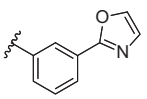	53 ± 24	5.9 ± 0.4	
17q	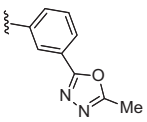	27 ± 8.3	–	
17r	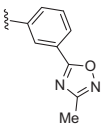	31 ± 6.3	–	
17s	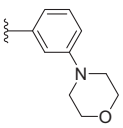	68 ± 6.3	12 ± 2.7	
17t	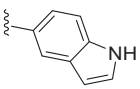	85 ± 6.5	5.9 ± 1.0	13.5 ± 3.5
17u	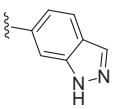	52 ± 8.3	–	
17v	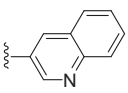	43 ± 3.3	–	
18a	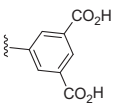	10 ± 5.3	–	
18b	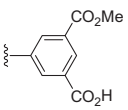	31 ± 14	–	
19a	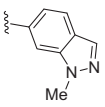	84 ± 9.1	3.1 ± 0.5	8.0 ± 3.9

[a]All values are the mean of three or more replicates ± SEM.
[b]No IC_{50} obtained due to limited solubility at higher concentrations.

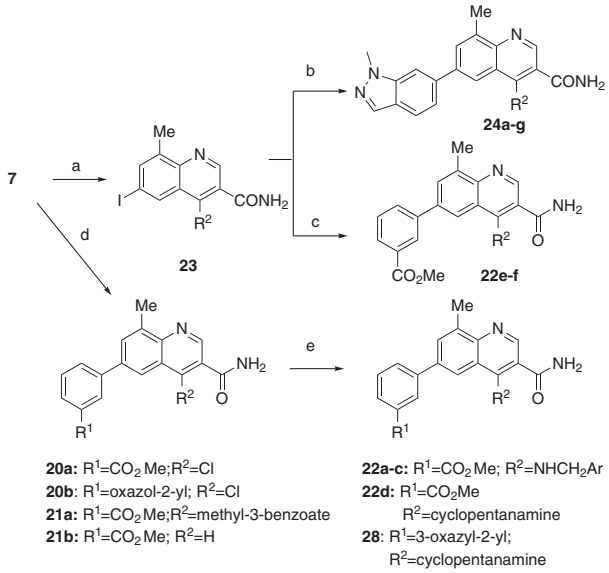

Scheme 3: Preparation of analogs exploring Region B (Reagents and conditions. (a) Various amines (R^2), MeCN, 80 °C, 24 h (61–80%) or various amines (R^2), MeCN, 145 °C, 25 min (59–80%). (b) 1-Methyl-1*H*-indazole-6-boronic acid, Na_2CO_3, $Pd(dppf)Cl_2$, dioxane, 130 or 145 °C, MW, 20 min (9–22%). (c) (3-(methoxycarbonyl) phenyl)boronic acid, Na_2CO_3, $Pd(dppf)Cl_2$, dioxane, 130–145 °C, MW, 20 min (7–12%). (d) (3-(methoxycarbonyl) phenyl)boronic acid or (3-(oxazol-2-yl)phenyl) boronic acid, Na_2CO_3, $Pd(dppf)Cl_2$, dioxane, 150 °C, MW, 10 min (**20a** (30%), **20b** (14%), (**21a** (5%), **21b** (2%)). (e) Various amines (R^2), MeCN, 80 °C, 48 h (10–40%)).

As shown in Table 3, compound activity is affected by the regiochemistry of the methoxy substituent on the R^2 group: *para* substitution is not tolerated (**24a**), whereas the *ortho* methoxy analog **24b** is only slightly less potent than **19a**. We observe that the ethyl analog **24d**, which is isosteric to **19a**, is just as potent. This led us to question the essentiality of this oxygen atom, although some sort of substitution at this position seems important (compare **19a** versus **24a** or **24g**).

Analogs of **17a** are sensitive to the spacing between the B region substituent and the rest of the molecule. Extending this spacing by an additional carbon (*e.g.,* **22a**) led to loss of activity. Removal of this substituent altogether resulted in a total loss of activity (**21b**). Finally, comparison of **17a** and the N-methylated analog **22e** reveals loss in activity.

Synthesis of analogs varying Regions C and D of **19a** is shown in Schemes 2 and 4. Reaction of **7** with NaH and iodomethane in DMF provided intermediates **25a-b** (Scheme 4). Heating of these intermediates with *m*-anisidine in acetonitrile afforded **26a-b**, which were subjected to Suzuki reaction to provide the Region C variants **27a-b**.

The variations at Region D were introduced at the beginning of the synthesis when the appropriate aniline **5** was used (Scheme 2). The methylindazole fragment was introduced in the last step via Suzuki chemistry to provide analogs **19a-c**.

As shown in Table 4, the primary amide in Region C is required; substitution with one or two methyl groups leads to dramatic loss of activity (**19a** versus **27a** and **27b**). Removal of the Region D methyl group leads to a ~4-fold loss in activity (**19a** versus **19b**), while extension to an ethyl group (*i.e.,* **19c**) is approximately equipotent.

The range of activity in this SAR study is relatively narrow, spanning potency differences of about 100-fold, although we were pleased that we were able to improve compound potency about eightfold from **3**. Inhibition of both TbrPDEB1 and B2 is required, although we have previously noted close correlation in TbrPDEB1 and B2 IC_{50} values (7). Therefore, we periodically obtained TbrPDEB2 IC_{50} values for compounds and tested against both PDEs prior to assessment in *T. brucei* cells. We note that, with the exception of one compound **10a**, those compounds tested against TbrPDEB2 showed IC_{50} values within ~2-fold of TbrPDEB1. Testing against human PDE4B unfortunately confirmed that these compounds remain extraordinarily potent inhibitors (Table 5). Nonetheless, testing of some of the most potent TbrPDEB1/B2 inhibitors does show cellular growth inhibition approximating the biochemical potency. One notable exception is the lead compound **3**; surprisingly, although this compound is a

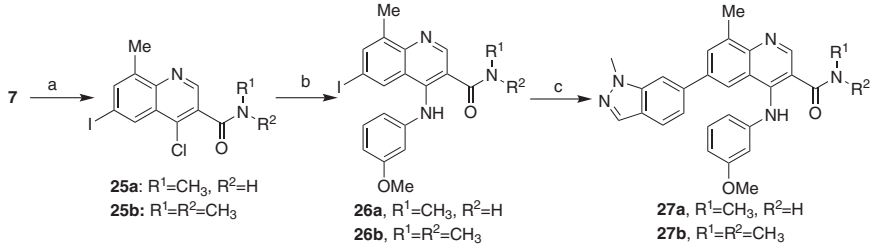

Scheme 4: Preparation of analogs **27** exploring Region C (Reagents and conditions. (a) NaH, DMF, 30 min, rt, then CH_3I, rt, overnight (52–100%). (b) 3-methoxyaniline, MeCN, 80 °C, overnight (40–60%). (c) 1-Methyl-1*H*-indazole-6-boronic acid, Na_2CO_3, $Pd(dppf)Cl_2$, dioxane, 160 °C, MW 20 min (8–17%)).

Table 3: Biochemical data for analogs exploring Region B[a]

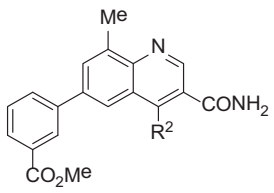

17, 21, 22

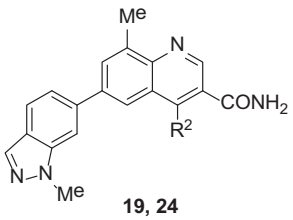

19, 24

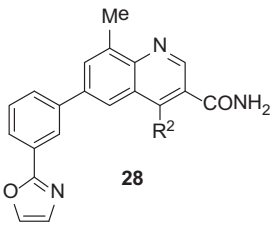

28

Compound	R^2	TbrPDEB1 (% inh)	TbrPDEB1 (IC_{50} μM)
17a	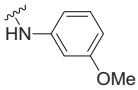	94 ± 3.5	6.4 ± 1.7
21a	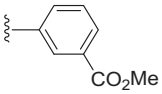	41 ± 5.8	–
21b		0	–
22a	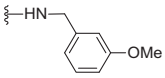	19 ± 6.6	–
22b	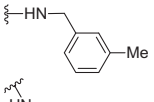	19 ± 4.2	–
22c		22 ± 20	28 ± 3.4
22d		80 ± 4.8	nd[b]
22e	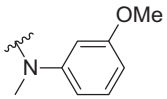	59 ± 3.6	–
22f	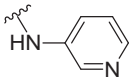	72 ± 14	26 ± 1.3
19a	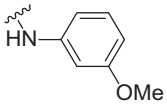	83.7 ± 9.1	3.8 ± 0.4
24a	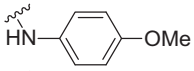	34 ± 0.3	–
24b	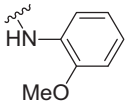	60 ± 16	7 ± 0.9
24c	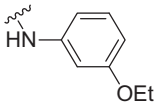	82 ± 12	4.2 ± 0.6
24d	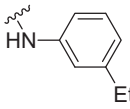	67 ± 7.5	3.5 ± 0.5

Table 3: continued

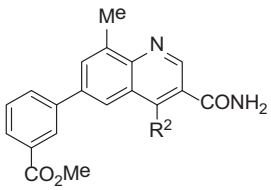

17, 21, 22

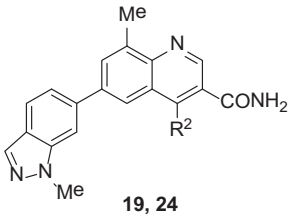

19, 24

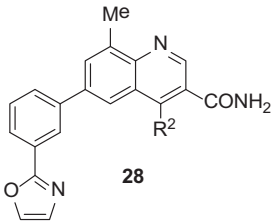

28

Compound	R^2	TbrPDEB1 (% inh)	TbrPDEB1 (IC_{50} μM)
24e	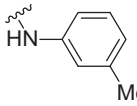	85 ± 11	3.5 ± 0.6
24f	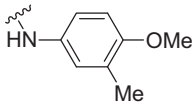	69 ± 16	3.7 ± 0.2
24g	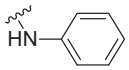	21 ± 6.5	–
28	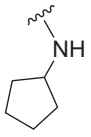	76 ± 2.2	5.9 ± 0.67

[a]All values are the mean of three or more replicates ± SEM.
[b]No IC_{50} obtained due to limited solubility at higher concentrations.

weak TbrPDEB1/B2 inhibitor, it inhibits cell growth with an EC_{50} of 7.8 uM. We presume this must be due to other mechanisms of inhibition operating in the cell.

We looked toward molecular modeling to help explain our observations, utilizing the recently published X-ray crystal structure of TbrPDEB1 to perform docking experiments of key analogs of **3**. The binding mode of a similar quinoline derivative in complex with the human PDE4B2B was reported in a crystal structure published by Lunniss and co-workers (19). This crystal structure reveals that the quinoline nitrogen of **3** interacts with the amide NH_2 of Gln874 and that the ligand amide NH_2 (Region C in Figure 1) interacts with carbonyl group of Asn825 residue (Figure 2A). Both residues (Gln874 and Asn825 in TbrPDEB1) are conserved between the human and parasite PDE and are therefore predicted to give similar interactions with this class of ligands. The amide carbonyl (Region C) is predicted to give an internal hydrogen bond with the NH group of the substituent occupying area B (Figures 1 and 2A).

The Region A substituents are predicted to point toward the N-terminus of an alpha-helix, which is slightly positively charged in consequence of the dipole moment (27). The fact that electron-rich substituents occupying Region A (*e.g.,* **11**, Figure 2A) display generally better potency values could therefore be explained by their favorable interaction with this dipole. Within the helix, an important key amino acid change between the human PDE4B and parasite PDE is Ser454 to Asn717 (Figure 2A, B)(19). The docking poses of compounds **11**, **17a,** and **17m** are shown in Figure 2B, highlighting the hydrogen bonds to the amide NH_2 of Asn717. In addition, the linker in the substituent in Region A appears to play an important role in placing the electron-rich substituent in contact with the Asn717 residue in the N-terminal helix. Woodrow *et al.* (16) previously described the detrimental effect of replacing the sulfone linker with a sulfide (such as in the case of **9a** versus **10a**), likely due to the ease of the sulfone to preorient the molecule in the proper conformation compared to the more flexible sulfide. We infer that the C-C linker-containing compounds must be able to preorient similarly to their sulfone congeners given the similar activity profile (*e.g.,* **10a** and **17a**).

The substituents in Region B are predicted to occupy the space near the magnesium ion (Figure 2A). Analysis of the crystal structure of hPDE4B2B shows that the *m*-methoxy substituent is located in the proximity of magnesium (~4 Å), indirectly interacting with the metal *via* intervening water molecules (Figure S1A). However, in the case of TbrPDEB1, we note the interesting observation that analogs with ethyl or methyl replacements of the *m*-methoxy group

Table 4: Exploring Regions C and D of **19**

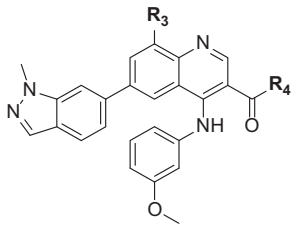

Compound	R_3	R_4	TbrPDEB1 (% inh)	TbrPDEB1 (IC_{50} μM)
19a	Me	NH_2	84 ± 9.1	3.1 ± 0.5
19b	H	NH_2	84 ± 2.4	12 ± 1.3
19c	Et	NH_2	79 ± 8.9	3.7 ± 0.5
27a	Me	$NHCH_3$	34 ± 11	–
27b	Me	NMe_2	22 ± 3.8	–

All values are the mean of three or more replicates ± SEM.

retain potency (compare **19a** with **24d** and **24e**), although an unsubstituted phenyl ring (**24g**) is detrimental for potency (Table 3**)**. Water prediction calculations (SZMAP v1.1.0, OpenEye Scientific Software) suggest that, in absence of a meta-position substitution in this phenyl group, there is a small, unoccupied cavity in the protein–ligand complex (Figure S1C). This unfavorable situation may explain the lack of activity of **24g**.

We predict the cyclopentyl-substituted compounds **22d** and **28** to orient in an alternative binding mode, accommodated by an alternative rotamer of Asn825 that is able to interact with the pyridine nitrogen of the ligand (Figure 2C) (28,29). We prepared these analogs, and while **28** is a 5.9-μM inhibitor of TbrPDEB1, **22d** was not sufficiently soluble to test in the dose–response experiment, although we observed the compound to inhibit TbrPDEB1 80% at 5 μM.

Methylation of the amide occupying Region C is detrimental for potency (compare **19a, 27a**, and **27b**, Table 4). This is consistent with the hypothesized essential H-bonding

Table 5: Biochemical and cellular characterization of the most potent TbrPDEB1 inhibitors

Compound	Reg. number	cLogP	TbrPDEB1 (IC_{50} μM)[a]	TbrPDEB2 (IC_{50} μM)[a]	hPDE4 (IC_{50} μM)[a]	*T. brucei* cell (EC_{50}, μM)[a]
3	**NEU-355**	4.33	24 ± 1.7	29.8 ± 7.5	7.9×10^{-6}	7.8 ± 2.5
10a	**NEU-356**	5.04	3.5 ± 0.3	15.1 ± 3.9	–	7.3 ± 0.97
17a	**NEU-433**	5.73	6.4 ± 1.7	6.2 ± 0.6	4.2×10^{-5}	7.0 ± 3.9
17t	**NEU-489**	5.82	5.9 ± 1.0	13.5 ± 3.5	–	5.6 ± 1.9
19a	**NEU-462**	5.17	3.1 ± 0.5	8.0 ± 3.9	8.3×10^{-5}	6.8 ± 0.82
19c	**NEU-528**	5.62	3.7 ± 0.5	5.6 ± 3.4	–	7.9 ± 2.7
24d	**NEU-542**	6.29	3.5 ± 0.5	12.1 ± 3.2	–	8.7 ± 1.8

[a]All values are the mean of three or more replicates ± SEM.

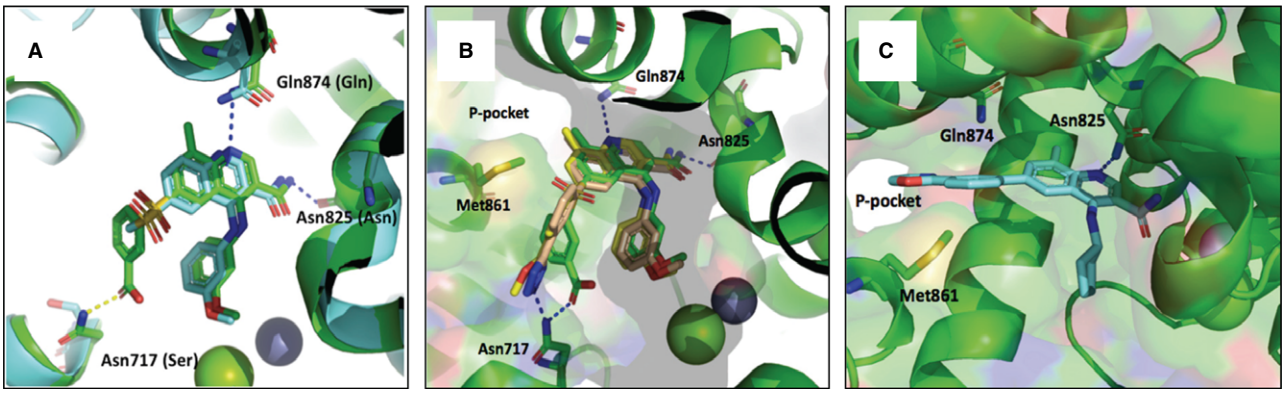

Figure 2: (A). Overlay of the crystal structure of the human phosphodiesterase 4B2B in complex with a quinoline inhibitor (PDB code: 3FRG, cyan carbon atoms) with the docked conformation of **11** in TbrPDEB1 (green carbon atoms). TbrPDEB1 residue numbering is used, with the corresponding hPDE4B residues in brackets. (B). Overlay of the docking poses of (i) **17a** (yellow carbon atoms), (ii) **11** (green carbon atoms), and (iii) **17m** (brown carbon atoms) in TbrPDEB1. (C). Docked conformation of **28** in TbrPDEB1. This pose was generated using FRED. The side chain of Asn825 has been flipped to allow a hydrogen bond of the amidic nitrogen with the pyridine nitrogen of the ligand. In all these figures, Mg^{2+} and Zn^{2+} are shown as green and gray spheres, respectively, and the interactions of the ligands with Gln 874, Asn 825, and Asn 717 are shown in blue dashed lines. The surface of the active site and the P-pocket can also be seen in B and C. Images generated using the PYMOL Molecular Graphics System, Version 1.5.0.4 Schrödinger, LLC.

interaction between this amide NH_2 and Asn825 (Figure 2A and B). Finally, the R^3 substituent (Region D) is predicted to occupy an area, adjacent to the 'parasite-' or 'P-pocket' (Figure 2B) (7,21), defined by the side chain of Met861 and the alpha-helix located at the back pocket of the active site. The presence of a methyl or ethyl group in Region D is predicted to increase potency by partially filling the P-pocket, and this potency improvement was confirmed experimentally as can be seen by comparing the potency values for compounds **19a**, **19b**, and **19c** in Table 4.

Discussion and Conclusions

We have applied a target repurposing approach to identify inhibitors of TbrPDEB1, an essential enzyme of the protozoan pathogen *T. brucei*. One of the advantages of this approach is the ability to launch optimization studies for new inhibitors with minimal upfront screening efforts. Indeed, our efforts to re-optimize chemotypes related to piclamilast (7,10), cilomilast (30), and now GSK-256066 for improved potency against TbrPDEB1 were launched by a broad assessment of 20 existing human PDE inhibitors (7). In this report, the SAR of the GSK-256066 chemotype was elaborated in a rapid fashion and provided improved analogs such as **10a**, **17a**, **17t**, **19a**, **19c,** and **24d**. This was possible by systematically studying the four regions of compound **3** (Figure 1) that we set out to explore. Our work revealed some general requirements needed for increased activity. First, for Region A, the most favorable functionalities were the meta substituted (e.g., ester, carboxylic acid, small heterocycles) aryls (e.g., **10a**, **11**, **17m**, **17o**, **17p**) or the methylindazole fragment (**19a**). This highlights that while Region A needs to be filled with lipophilic aromatic cores, this is not sufficient for activity. More important is a requirement for hydrogen acceptor groups that may interact with Asn717 (Figure 2B). Furthermore, for Region B, we discovered that substituted aryls in the meta-position with groups such as methyl, ethyl, methoxy, or ethoxy (i.e., **24e**, **24d**, **17a** and **24c**) are preferred for increased activity, as there is a small unoccupied cavity in the protein–ligand complex that we posit is now filled by these lipophilic groups (Figure S1C). For Region C, the amide functionally was shown to be essential as it interacts with Asn825, which is present in both hPDE4 and TbrPDEB1 (shown in Figure 2A). Lastly, for Region D, we show that by occupying the P-pocket by a methyl (**19a**) or ethyl substituent (**19c**), we observe an increase in activity (Figure 2B). This region would benefit from additional exploration, although this is synthetically the most challenging part of the molecule to vary. In the end, our medicinal chemistry efforts provided compound **19a**, which is 6.5-fold more active in the TbrPDEB1 biochemical assay, 10.5-fold less potent against hPDE4, and show modest potency against *T. brucei* cells.

Unfortunately, the compounds we have identified still retain significant (subnanomolar) potency against human PDE4 (e.g., **19a** IC_{50} = 0.083 nM). Although this represents a slight improvement in overall selectivity, more must be done to improve selectivity for a new HAT therapeutic. For us, and for others (17,18), this appears to be a significant issue that has yet to be overcome, though with recent structural biology reports of TbrPDEB1 (21), we expect that understanding about the ligand–target interactions that drive selectivity will become more clear in the near future.

Importantly, in most cases, the structure–activity relationships we observe are consistent with the expected binding modality of this chemotype, based on previous structural biology reports of **3** bound to hPDE4B (16). For example, the requirement for an unsubstituted 3-quinoline carboxamide moiety is retained. On the other hand, we have made a surprising observation regarding the importance of the *m*-methoxy substituent in Region B: in hPDE4, this functionality provides ~7-fold potency over an alkyl group at this position (16), presumably by interacting with the catalytic metal ion via intervening water molecules. On the other hand, in the parasite enzyme, replacement of this methoxy group with an isosteric ethyl group shows surprisingly good activity (compare **19a** with **24d**, which have equivalent TbrPDEB1 and cellular potency, Table 5).

Acknowledgments

This work was funded by the National Institutes of Health (R01AI082577). We are grateful to Dr Emanuele Amata for helpful discussions. A free academic license to OpenEye Scientific Software and ChemAxon for their suites of programmes is gratefully acknowledged.

Conflict of Interest

The authors declare that no conflict of interest exists.

References

1. Savioli L., Daumerle D. Sustaining the drive to overcome the global impact of neglected tropical diseases. World Health Organization 2013. Available from: http://apps.who.int/iris/bitstream/10665/77950/1/9789241564540_eng.pdf.
2. Priotto G., Kasparian S., Mutombo W., Ngouama D., Ghorashian S., Arnold U., Ghabri S. *et al.* (2009) Nifurtimox-eflornithine combination therapy for second-stage African *Trypanosoma brucei gambiense* trypanosomiasis: a multicentre, randomised, phase III, non-inferiority trial. Lancet;374:56–64.
3. Nok A.J. (2003) Arsenicals (melarsoprol), pentamidine and suramin in the treatment of human African trypanosomiasis. Parasitol Res;90:71–79.
4. Pollastri M.P., Campbell R.K. (2011) Target repurposing for neglected diseases. Future Med Chem;3:1307–1315.

5. Ochiana S.O., Pandarinath V., Wang Z., Kapoor R., Ondrechen M.J., Ruben L., Pollastri M.P. (2013) The human Aurora kinase inhibitor danusertib is a lead compound for anti-trypanosomal drug discovery via target repurposing. Eur J Med Chem;62:777–784.
6. Patel G., Karver C.E., Behera R., Guyett P.J., Sullenberger C., Edwards P., Roncal N.E., Mensa-Wilmot K., Pollastri M.P. (2013) Kinase scaffold repurposing for neglected disease drug discovery: discovery of an efficacious, lapatanib-derived lead compound for trypanosomiasis. J Med Chem;56:3820–3832.
7. Bland N.D., Wang C., Tallman C., Gustafson A.E., Wang Z., Ashton T.D., Ochiana S.O. *et al.* (2011) Pharmacological validation of *Trypanosoma brucei* phosphodiesterases B1 and B2 as druggable targets for African sleeping sickness. J Med Chem;54:8188–8194.
8. Ochiana S.O., Gustafson A., Bland N.D., Wang C., Russo M.J., Campbell R.K., Pollastri M.P. (2012) Synthesis and evaluation of human phosphodiesterases (PDE) 5 inhibitor analogs as trypanosomal PDE inhibitors. Part 2. Tadalafil analogs. Bioorg Med Chem Lett;22:2582–2584.
9. Wang C., Ashton T.D., Gustafson A., Bland N.D., Ochiana S.O., Campbell R.K., Pollastri M.P. (2012) Synthesis and evaluation of human phosphodiesterases (PDE) 5 inhibitor analogs as trypanosomal PDE inhibitors. Part 1. Sildenafil analogs. Bioorg Med Chem Lett;22:2579–2581.
10. Woodring J.L., Bland N.D., Ochiana S.O., Campbell R.K., Pollastri M.P. (2013) Synthesis and assessment of catechol diether compounds as inhibitors of trypanosomal phosphodiesterase B1 (TbrPDEB1). Bioorg Med Chem Lett;23:5971–5974.
11. Setter S.M., Iltz J.L., Fincham J.E., Campbell R.K., Baker D.E. (2005) Phosphodiesterase 5 inhibitors for erectile dysfunction. Ann Pharmacother;39:1286–1295.
12. Greulich T., Koczulla A.R., Vogelmeier C. (2012) Chronic obstructive pulmonary disease: new pharmacotherapeutic options. Internist (Berl);53:1364–1370.
13. Maiga M., Agarwal N., Ammerman N.C., Gupta R., Guo H., Maiga M.C., Lun S., Bishai W.R. (2012) Successful shortening of tuberculosis treatment using adjuvant host-directed therapy with FDA-approved phosphodiesterase inhibitors in the mouse model. PLoS ONE;7:e30749.
14. Yano M., Kohno M., Ohkusa T., Mochizuki M., Yamada J., Hisaoka T., Ono K., Tanigawa T., Kobayashi S., Matsuzaki M. (2000) Effect of milrinone on left ventricular relaxation and Ca(2 +) uptake function of cardiac sarcoplasmic reticulum. Am J Physiol Heart Circ Physiol;279:H1898–H1905.
15. Oberholzer M., Marti G., Baresic M., Kunz S., Hemphill A., Seebeck T. (2007) The *Trypanosoma brucei* cAMP phosphodiesterases TbrPDEB1 and TbrPDEB2: flagellar enzymes that are essential for parasite virulence. FASEB J;21:720–731.
16. Woodrow M.D., Ballantine S.P., Barker M.D., Clarke B.J., Dawson J., Dean T.W., Delves C.J. *et al.* (2009) Quinolines as a novel structural class of potent and selective PDE4 inhibitors. Optimisation for inhaled administration. Bioorg Med Chem Lett;19:5261–5265.
17. de Koning H.P., Gould M.K., Sterk G.J., Tenor H., Kunz S., Luginbuehl E., Seebeck T. (2012) Pharmacological validation of *Trypanosoma brucei* phosphodiesterases as novel drug targets. J Infect Dis;206:229–237.
18. Orrling K.M., Jansen C., Vu X.L., Balmer V., Bregy P., Shanmugham A., England P. *et al.* (2012) Catechol pyrazolinones as trypanocidals: fragment-based design, synthesis, and pharmacological evaluation of nanomolar inhibitors of trypanosomal phosphodiesterase B1. J Med Chem;55:8745–8756.
19. Lunniss C.J., Cooper A.W., Eldred C.D., Kranz M., Lindvall M., Lucas F.S., Neu M., Preston A.G., Ranshaw L.E., Redgrave A.J., Ed Robinson J., Shipley T.J., Solanke Y.E., Somers D.O., Wiseman J.O. (2009) Quinolines as a novel structural class of potent and selective PDE4 inhibitors: optimisation for oral administration. Bioorg Med Chem Lett;19:1380–1385.
20. Baldwin I.R., Barker M.D., Dean A.W., Eldred C.D., Evans B., Gough S.L., Guntrip S.B. *et al.* (2004) Preparation of quinoline derivatives as phosphodiesterase inhibitors. WO2004103998A1.
21. Jansen C., Wang H., Kooistra A.J., de Graaf C., Orrling K.M., Tenor H., Seebeck T., Bailey D., de Esch I.J., Ke H., Leurs R. (2013) Discovery of novel *Trypanosoma brucei* phosphodiesterase B1 inhibitors by virtual screening against the unliganded TbrPDEB1 crystal structure. J Med Chem;56:2087–2096.
22. Surry D.S., Buchwald S.L. (2008) Biaryl phosphane ligands in palladium-catalyzed amination. Angew Chem;47:6338–6361.
23. Schopfer U., Schlapbach A. (2001) A general palladium-catalyzed synthesis of aromatic and heteroaromatic thioethers. Tetrahedron;57:3069–3073.
24. Buckman B., Nicholas J.B., Beigelman L., Serebryany V., Stoycheva A.D., Thrailkill T., Seiwert S.D. (2011) Preparation of macrocyclic peptides, especially proline-containing peptides, as inhibitors of hepatitis C virus replication for treating hepatitis C infection and liver fibrosis. WO2011038293A1.
25. Wu W.-L., Burnett D.A., Stamford A.W., Cumming J.N., Bennett C.E., Gilbert E.J., Peng X., Scott J.D., Yu Y. (2012) Preparation of 5-substituted iminothiazines and their mono- and dioxides as BACE inhibitors. WO2012139425A1.
26. Young J., Czako B., Altman M., Guerin D., Martinez M., Rivkin A., Wilson K., Lipford K., White C., Surdi L., Chichetti S., Daniels M.H., Ahearn S.P., Falcone D., Osimboni E. (2011) Pyridazinones as tyrosine kinase inhibitors and their preparation and use in the treatment of cancer. WO2011084402A1.
27. Wada A. (1976) The alpha-helix as an electric macrodipole. Adv Biophys;1–63.
28. Higman V.A., Boyd J., Smith L.J., Redfield C. (2004) Asparagine and glutamine side-chain conformation in solution and crystal: a comparison for hen egg-white

lysozyme using residual dipolar couplings. J Biomol NMR;30:327–346.
29. Word J.M., Lovell S.C., Richardson J.S., Richardson D.C. (1999) Asparagine and glutamine: using hydrogen atom contacts in the choice of side-chain amide orientation. J Mol Biol;285:1735–1747.
30. Amata E., Bland N.D., Hoyt C.T., Settimo L., Campbell R.K., Pollastri M.P. (2014) Repurposing human phosphodiesterase 4 inhibitors for neglected tropical diseases. 1. Design, synthesis and evaluation of cilomilast analogues as Trypanosoma brucei phosphodiesterase B1 (TbrPDEB1) inhibitors. Bioorg Med Chem Lett;24:4084–4089.
31. Duplantier A.J., Bachert E.L., Cheng J.B., Cohan V.L., Jenkinson T.H., Kraus K.G., McKechney M.W., Pillar J.D., Watson J.W. (2007) SAR of a Series of 5,6-Dihydro-(9H)-pyrazolo[3,4-c]-1,2,4-triazolo[4,3-α]pyridines as Potent Inhibitors of Human Eosinophil Phosphodiesterase. J Med Chem;50:344–349.
32. Ehrman T.M., Barlow D.J., Hylands P.J. (2010) *In silico* search for multi-target anti-inflammatories in Chinese herbs and formulas. Bioorg Med Chem;18: 2204–2218.

Supporting Information

Additional Supporting Information may be found in the online version of this article:

Appendix S1. The screening data has been made freely available as a shared data set at www.collaborativedrugdiscovery.com.
Figure S1. (A). Hydrogen bond network near the head group region as seen in the crystal structure of the human phosphodiesterase 4B2B in complex with a quinoline Inhibitor (PDB code: 3FRG, cyan carbon atoms).